Assessing Atmospheric Response to Surface Forcing in the Observations. Part II: Cross Validation of Seasonal Response Using GEFA and LIM

ZHENGYU LIU

Laboratory for Climate and Ocean-Atmosphere Studies, School of Physics, Peking University, Beijing, China, and Center for Climatic Research, University of Wisconsin—Madison, Madison, Wisconsin

LEI FAN

Laboratory of Physical Oceanography, Ocean University of China, Qingdao, China

SANG-IK SHIN

College of Marine Sciences, University of South Florida, Tampa, Florida

QINYU LIU

Laboratory of Physical Oceanography, Ocean University of China, Qingdao, China

(Manuscript received 4 October 2011, in final form 20 April 2012)

ABSTRACT

The authors compared the assessment of the seasonal cycle of the atmospheric response to surface forcing in three statistical methods, generalized equilibrium feedback analysis (GEFA), linear inverse modeling (LIM), and fluctuation–dissipation theorem (FDT). These methods are applied to both a conceptual climate model and the observation. It is found that LIM and GEFA are able to reproduce the major features of the seasonal response consistently, whereas FDT tends to generate a bias of the phase of the seasonal cycle. The success of LIM and GEFA for the assessment of the seasonal response is due to the slowly varying nature of the annual cycle relative to the atmospheric response time. Therefore, the authors recommend GEFA and LIM as two independent methods for the assessment of the seasonal atmospheric response in the observation.

1. Introduction

A robust assessment of the atmospheric response to surface forcing in the observation is critical for our understanding of climate feedbacks. Because of the complex nature of ocean–atmosphere feedback[1] and the limited observations, a statistical assessment is usually subject to substantial uncertainty. It is therefore desirable to develop independent statistical methods for cross validation. Recently, Liu et al. (2012, hereafter Part I) compared three methods for the assessment of the annual mean atmospheric response to multiple SST forcings in the observation: generalized equilibrium feedback analysis (GEFA; Frankignoul et al. 1998; Liu et al. 2008), linear inverse modeling (LIM; Penland and Sardeshmukh 1995; Newman et al. 2009) and fluctuation–dissipation theorem (FDT; Leith 1975; Bell 1980). It is found that the three methods produce highly consistent annual mean atmospheric responses and therefore can be used for the cross validation of the major features of the atmospheric response to surface forcing in the observation.

This paper extends Part I to examine the seasonal response. The application of the statistical assessment to the seasonal cycle of the atmospheric response poses further challenges. First, given the same length of data, the effective sample size is reduced by a factor of 4 (12) for the response of each season (calendar month). Furthermore, unlike GEFA, which can be applied directly to assess the seasonal cycle of the response, the feasibility of

---

[1] Land–atmosphere feedback can be discussed similarly.

Corresponding author address: Zhengyu Liu, 1225 W. Dayton St., Madison, WI 53706.
E-mail: zliu3@wisc.edu

LIM and FDT for the assessments of the seasonal cycle of response is unclear. For LIM, cyclostationary methods, such as the fixed-phase and the phase-smoothed methods, have been used to study the eigenmodes of the temporal evolution of a seasonally varying system (e.g., Hasselmann and Barnett 1981; Blumenthal 1991; OrtizBreviá 1997). However, the feasibility of these methods on the assessment of the seasonal feedback among different components has not been studied, especially regarding the sampling error. For FDT, to our knowledge, there has been no study on its application to a seasonally varying system and therefore its application on seasonal response remains even more questionable. Here, we will show that LIM can still provide an accurate assessment of the seasonal cycle of the feedback response in the observation, comparable with GEFA, whereas FDT tends to produce a bias in the phase of the seasonal cycle. The ability for LIM to assess the seasonal response is due to the slow-varying nature of the seasonal cycle relative to the time scales of the coupled system, especially the fast atmosphere. As such, GEFA and LIM can be used as a cross validation for the seasonal atmospheric response in the observation. This paper is arranged similar to Part I. In section 2, we briefly discuss these methods. In section 3, we compare these methods in an idealized model. In section 4, we will compare the assessment of the seasonal atmospheric response in the observation using LIM and GEFA. A summary is given in section 5.

2. GEFA, LIM, and FDT

a. Stationary system

We first briefly review the three methods. Assume[2] that the coupled ocean–atmosphere system can be described by a set of linear, stochastic dynamic system as

$$\frac{d\mathbf{x}}{dt} = \mathbf{A_{xx}}\mathbf{x} + \mathbf{A_{xy}}\mathbf{y} + \mathbf{n_x} \quad \text{and} \quad (2.1a)$$

$$\frac{d\mathbf{y}}{dt} = \mathbf{A_{yx}}\mathbf{x} + \mathbf{A_{yy}}\mathbf{y} + \mathbf{n}_y, \quad (2.1b)$$

where $\mathbf{x}(t)$ is an atmospheric field; $\mathbf{y}(t)$ is an SST forcing field; and $\mathbf{n_x}$ and $\mathbf{n}_y$ are stochastic climate noises in the atmosphere and ocean, respectively. We further assume the coupled system is stationary such that the submatrices $\mathbf{A_{**}}$ are all time independent. One key feature of the coupled ocean–atmosphere system is a time-scale separation: the atmosphere response has the time scale of days to weeks, much faster than the slow SST variability of time scales of months. This multiple time scale can lead to significant simplifications not only in the dynamics but also in the statistical assessment of the coupled climate system. Averaged over a time scale longer than the atmospheric persistence time (days), the atmospheric response to SST variability (2.1a) can be approximated as a quasi-equilibrium response (see Part I for more details)

$$\mathbf{A_{xx}}\bar{\mathbf{x}} + \mathbf{A_{xy}}\bar{\mathbf{y}} + \bar{\mathbf{n}}_\mathbf{x} = 0, \quad (2.2)$$

where the overbar represents a time mean. Denoting

$$\mathbf{B} = -\mathbf{A_{xx}^{-1}}\mathbf{A_{xy}} \quad (2.3)$$

and $\bar{\mathbf{n}} = -\mathbf{A_{xx}^{-1}}\bar{\mathbf{n}}_\mathbf{x}$, we have from (2.2)

$$\bar{\mathbf{x}}(t) = \mathbf{B}\bar{\mathbf{y}}(t) + \bar{\mathbf{n}}(t), \quad (2.4)$$

where $\mathbf{B}$ is the so-called feedback matrix, $\mathbf{B}\bar{\mathbf{y}}(t)$ is the quasi-equilibrium atmospheric response to SST forcing, and $\bar{\mathbf{n}}(t)$ is the internal atmospheric variability that is generated independent of SST forcing. Our objective is to estimate $\mathbf{B}$ from the observed atmosphere $\mathbf{x}(t)$ and ocean $\mathbf{y}(t)$.

As a variant of the regression approach (see Part I), GEFA is a multivariate generalization of the univariate feedback analysis of Frankignoul et al. (1998) (Liu et al. 2008). Because the SST variability cannot be forced by the atmospheric internal variability of later times, we have

$$\mathbf{C_{\bar{n}\bar{y}}}(\tau) = \langle \bar{\mathbf{n}}(t), \ \bar{\mathbf{y}}(t-\tau) \rangle = 0 \quad (\tau > \tau_n), \quad (2.5)$$

where $\langle \ \rangle$ is the covariance and τ is a lag longer than the persistence time of the atmospheric internal variability τ_n. The feedback matrix $\mathbf{B}$ can then be derived after a right multiplication by the lagged SST as

$$\mathbf{B} = \mathbf{C_{\bar{x}\bar{y}}}(\tau)\mathbf{C_{\bar{y}\bar{y}}^{-1}}(\tau). \quad (2.6)$$

For a finite sample size $t = 1, \ldots, T$, the sample covariance is calculated as

---

[2] For real-world application, this linear dynamic approximation is not obviously valid a priori. In particularly, synoptic atmospheric dynamics at subdaily and daily time scales are strongly nonlinear and exhibit chaotic behavior at climate time scales. However, a sufficiently long time average (relative to the nonlinear atmospheric dynamics: e.g., days) could render the high-frequency nonlinear dynamics to stochastic noise according to the central limit theorem (Gardiner 1997). Thus, coupled system may be approximated as a linear dynamic system driven by stochastic forcing.

$$\mathbf{C_{xy}}(\tau) = \frac{1}{T} \sum_{t=1}^{T} [\mathbf{x}(t) - \tilde{\mathbf{x}}(t)][\mathbf{y}(t - \tau) - \tilde{\mathbf{y}}(t - \tau)]^{\mathrm{T}},$$
$$(2.7)$$

where the T superscript is the transpose and

$$\tilde{\mathbf{x}}(t) = \frac{1}{T} \sum_{t=1}^{T} \mathbf{x}(t)$$

represents the sample mean.

Although GEFA takes advantage of the multiple time scales of the coupled system and approximate the atmospheric response to SST as a quasi-equilibrium response (2.2) or (2.4), LIM and FDT extract the atmospheric response to SST from the transient evolution of the coupled system, with the temporal atmospheric response resolved explicitly. We can first estimate the system submatrices $\mathbf{A_{xx}}$ and $\mathbf{A_{xy}}$ in (2.1a) using LIM and then derive the feedback matrix $\mathbf{B}$ using (2.3) (Alexander et al. 2008; Newman et al. 2009). The system submatrices can be derived by combining the atmospheric and oceanic fields together as a single climate field

$$\mathbf{z} = \begin{bmatrix} \mathbf{x} \\ \mathbf{y} \end{bmatrix}$$

and rewrite the coupled Eqs. (2.1a) and (2.1b) as

$$\frac{d\mathbf{z}}{dt} = \mathbf{A}\mathbf{z} + \hat{\mathbf{n}}, \qquad (2.8)$$

where

$$\mathbf{A} = \begin{bmatrix} \mathbf{A_{xx}} & \mathbf{A_{xy}} \\ \mathbf{A_{yx}} & \mathbf{A_{yy}} \end{bmatrix}, \quad \hat{\mathbf{n}} = \begin{bmatrix} \mathbf{n_x} \\ \mathbf{n_y} \end{bmatrix}. \qquad (2.9)$$

If the $\mathbf{A}$ is independent of time and the noise is Gaussian, the optimal solution for a lead time τ is (Penland 1989)

$$\mathbf{z}(t + \tau) = \mathbf{G}(\tau)\mathbf{z}(t), \qquad (2.10a)$$

with the propagator $\mathbf{G}(\tau)$ as

$$\mathbf{G}(\tau) = \exp(\mathbf{A}\tau). \qquad (2.10b)$$

Thus, the propagator can be estimated by a right multiplication of $\mathbf{z}^T(t)$ on (2.10a) in LIM as

$$\mathbf{G}(\tau) = \mathbf{C_{zz}}(\tau)\mathbf{C_{zz}^{-1}}(0). \qquad (2.11a)$$

Combining (2.10b) and (2.11a), we have the LIM estimator for the system matrix $\mathbf{A}$ as

$$\mathbf{A} = \tau^{-1} \ln\{\mathbf{C_{zz}}(\tau)\mathbf{C_{zz}^{-1}}(0)\}. \qquad (2.11b)$$

Finally, the system matrix $\mathbf{A}$ can also be estimated using a modified formula relevant to FDT (Leith 1975; Bell 1980). Once again, assuming $\mathbf{A}$ is independent of time, taking the exponential on both sides of (2.11b) and then integrating over all the lags, we have the FDT estimator as (Kirk-Davidoff 2009)

$$-\mathbf{A}^{-1} = \int_0^{\tau} \mathbf{C_{zz}}(\tau')\mathbf{C_{zz}^{-1}}(0) \, d\tau', \quad \tau \to \infty. \quad (2.12)$$

If the sample size is sufficiently large, and the linear dynamic system is stationary (time-independent $\mathbf{A}$), the three methods, GEFA in (2.6), LIM in (2.11b) and (2.3), and FDT in (2.12) and (2.3), will give the same feedback matrix $\mathbf{B}$. For a limited sample size relevant to climate observations, however, the estimation of the system matrix $\mathbf{A}$ is usually subject to large sampling errors (e.g., Gritsun and Branstator 2007). Nevertheless, for a realistic sample size (decades), Part I demonstrated that the feedback matrix $\mathbf{B}$ can still be estimated accurately in LIM and FDT as in GEFA, because of a cancelation of the sampling errors between the submatrices $\mathbf{A_{xx}}$ and $\mathbf{A_{xy}}$ in deriving $\mathbf{B}$ from (2.3).

b. Seasonally varying system

Now, we consider the seasonal response. Suppose the dynamic system is modulated by the seasonality of the system matrix $\mathbf{A}(t)$. This will lead to a seasonally dependent feedback matrix $\mathbf{B}(t)$. Suppose k is a specific phase of the annual cycle: say, a calendar month (week or day). Then 1 yr has a total of K phases, and $\Delta t = 1 \text{ yr}/K$ is the time increment between each phase. The periodicity of the system matrix gives

$$\mathbf{A}_k \equiv \mathbf{A}(k\Delta t) = \mathbf{A}[(K + k)\Delta t] \equiv \mathbf{A}_{K+k}, \quad k = 1, 2, \ldots, K,$$
$$(2.13)$$

and similarly $\mathbf{B}_k = \mathbf{B}_{K+k}$. Because the seasonal cycle is much longer than the atmospheric response time, the quasi-equilibrium response (2.2) or (2.4) should still be approximately valid. Therefore, in principle, the seasonal evolution of the feedback matrix $\mathbf{B}_k$ can still be estimated using GEFA as in the case of time-independent $\mathbf{B}$ in (2.6), except with the covariance now calculated centered around the specific phase; that is, (2.6) and (2.7) are modified as

$$\mathbf{B}_k = \mathbf{C}_{\overline{\mathbf{x}}_k \overline{\mathbf{y}}_k}(\tau)\mathbf{C}_{\overline{\mathbf{y}}_k \overline{\mathbf{y}}_k}^{-1}(\tau) \qquad (2.14)$$

with the sample covariance for, say, $\mathbf{C}_{\mathbf{x}_k \mathbf{y}_k}(\tau)$ as

$$\mathbf{C}_{\mathbf{x}_k \mathbf{y}_k}(\tau) = \frac{1}{M} \sum_{m=0}^{M-1} \{\mathbf{x}[(mK + k)\Delta t] - \hat{\mathbf{x}}\}\{\mathbf{y}[(mK + k - \tau)\Delta t] - \hat{\mathbf{y}}\}^T, \qquad (2.15)$$

where

$$\hat{\mathbf{x}} = \frac{1}{M} \sum_{m=0}^{M-1} \mathbf{x}[(mK + k)\Delta t]$$

represents the sample mean across different years. Here, we have assumed that the total sample size T contains M years of data: that is, $T = MK\Delta t$.

LIM and FDT, however, are more complex. Strictly speaking, with a time-dependent system matrix $\mathbf{A}$, the optimal solution (2.10a) and (2.10b) to the coupled system is no longer valid. Therefore, it is unclear if the seasonally varying $\mathbf{A}$ (and in turn the feedback matrix $\mathbf{B}$) can still be estimated accurately using the LIM estimator (2.11b) or the FDT estimator (2.12). Physically, although the seasonal cycle is much longer than the atmospheric response time, it can be comparable with the oceanic time scale. Therefore, it is unclear if the seasonal dependence of the system matrix $\mathbf{A}$ can be estimated accurately using LIM or FDT. Here, we test an intuitive and simple-minded approach. Because the seasonal cycle is much longer than the atmospheric response time, we may speculate that it is still possible for LIM and FDT to give a reasonable estimation of the feedback matrix as in the stationary case. Therefore, we will still use the LIM estimator (2.11b), modified for the seasonally varying case, as

$$\mathbf{A}_k = \tau^{-1} \ln\{\mathbf{C}_{\mathbf{z}_k \mathbf{z}_k}(\tau)\mathbf{C}_{\mathbf{z}_k \mathbf{z}_k}^{-1}(0)\}, \qquad (2.16)$$

where the covariance for phase k is calculated using the same phase but different years, as in (2.15). This LIM estimator is reminiscent of the fixed-phase method in previous LIM studies but directly using the continuous solution (2.15). In the same spirit, the FDT estimator is modified as

$$-\mathbf{A}_k^{-1} = \int_0^\tau \mathbf{C}_{\mathbf{z}_k \mathbf{z}_k}(\tau')\mathbf{C}_{\mathbf{z}_k \mathbf{z}_k}^{-1}(0) \, d\tau', \quad \tau \to \infty. \quad (2.17)$$

In previous LIM applications to a seasonally varying system, two methods are used: the fixed-phase and phase-smoothed methods (Hasselmann and Barnett 1981; OrtizBreviá 1997). Both methods, however, apply readily only to the finite difference form of an AR(1) system, which is an approximation to the continuous system (2.8). Furthermore, these studies have focused on the transient evolution with the focus on the estimation of the propagator

$\mathbf{G}(\tau)$ and its eigenmodes. However, the estimation of the system matrix $\mathbf{A}$ is likely to be more difficult and more sensitive to sampling error than the propagator, because of the log function. In any case, we have attempted to derive some approximate LIM estimators for the seasonally varying system matrix $\mathbf{A}_k$, following the idea of the fixed-phase method in the finite difference form of (2.8). However, there is no clear evidence the sampling error of these methods is smaller than the simple-minded Eq. (2.16). Indeed, in some sense, the approximate LIM estimator (2.16) is in the spirit of the fixed-phase method of previous LIM studies but directly using the continuous solution (2.15). As for FDT, we have yet to find an alternative estimator other than the estimator (2.17).

3. An idealized model study

We first study the seasonal assessment in an idealized coupled model similar to Barsugli and Battisti (1998), which can be described in nondimensional equations as

$$\frac{dx}{dt} = -ax + by + n \quad \text{and} \qquad (3.1a)$$

$$M\frac{dy}{dt} = cx - dy. \qquad (3.1b)$$

The parameters are chosen as $a = 1.3$, $b = 1 + 0.2 \sin(t2\pi/T)$, $c = 1$, $d = 1$, $M = 10$. Here, n is a Gaussian white noise. A unit time $t = 1$ corresponds to a nominal time of ~ 4 days. Therefore, the atmospheric response time scale to a given SST anomaly is $\sim 1/a \sim 3$ days and the oceanic response time scale to a given atmospheric forcing is $M/d \sim 40$ days or ~ 1–2 months. The coupled system has a decorrelation time of 1 week for the atmosphere and 4–5 months for SST (not shown), comparable with the observation. The seasonal cycle of the atmospheric response is prescribed in the parameter b, where $T \sim 90$ corresponds to ~ 1 yr. With the application to the present observation in mind, the model is integrated for 60 yr for each simulation, using the Euler forward scheme with a time step of 0.05, with the noise generated using a Gaussian random generator at each time step. To assess the sampling error, an ensemble of 50 simulations is used. (The results are similar for larger ensemble sizes.) Because the GEFA estimation of the seasonal cycle is straightforward using (2.14), we will focus on LIM and FDT below.
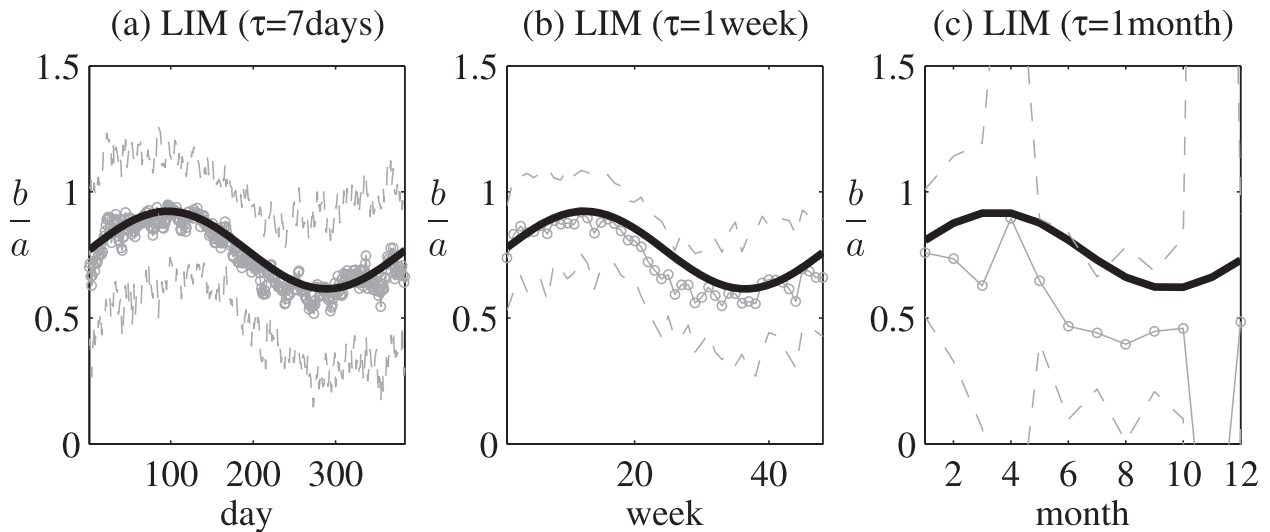
FIG. 1. The direct LIM estimation of the feedback parameter b/a with an annual cycle in the idealized model, for each calendar (a) day, (b) week, and (c) month, using daily, weekly, and monthly data, respectively. The thick solid line is the truth, the thin solid line with circles is the 50-ensemble mean, and the dashed line is the ensemble spread (stand deviation).

a. LIM

First, we confirmed one major finding of Part I about LIM. With a finite sample size here (about $\sim10^2$–10^3 atmospheric response time), the sampling error of the feedback parameter $B = b/a$ is reduced substantially relative to the coefficients a and b themselves, due to the cancelation of a common factor in the sampling error in a and b. As a result, **B** is not sensitive to the lag of estimation (see Fig. 3). Therefore, unless otherwise specified, we only show LIM results with a lag of ~1 week.

For climate applications, it is usually desirable to estimate the feedback parameter **B** of a specific calendar month (or season). However, for a better understanding of the LIM estimation, we will first examine the LIM estimation in daily, weekly, and monthly data, using the simplest method called the direct method here. For the direct estimation of the feedback parameter B_k of a specific phase k (calendar day, week, or month), the covariance in the LIM Eq. (2.11b) is calculated centered at the phase k as in Eq. (2.16). For example, for the estimation of the daily feedback parameter at day 150, the daily data of day 150 of each year will be used to calculate the covariance at lag 0 and the daily data of day 149 will then be used to calculate the lag 1-day covariance. Figure 1 shows the direct estimation of the seasonal cycles of the feedback parameter using daily, weekly, and monthly data. The estimated daily feedback parameter recovers well the true seasonal cycle in the ensemble mean, with an RMSE of ~0.05, confirming the unbiased estimation of LIM on the seasonal cycle for a sufficiently

large sample size (Fig. 1a). As the sample size is increased from 1×60 yr to 5×60 yr, 10×60 yr, 30×60 yr, 50×60 yr, and 100×60 yr, our further experiments show that the RMSE (correlation) of the ensemble mean estimation of the seasonal cycle is reduced (increased) from 0.25 (~0.4) to 0.13 (0.67), 0.09 (0.79), 0.055 (0.91), 0.045 (0.94), and 0.035 (0.97), respectively. Therefore, about 10×60 yr = 600 yr of data are needed to reduce the sampling error significantly below the amplitude of the current seasonal cycle signal ($0.2/1.3 \sim 0.15$) and with a correlation over ~0.8. The sampling error is large for each estimation of a sample size of 60 yr such that the ensemble spread (measured by the standard deviation averaged over the year) is 0.28, greater than the amplitude of the seasonal cycle, 0.15. This large sampling error renders the direct daily estimation rather inaccurate.

The large sampling error in the direct daily estimation is due partly to the large noise in the daily data. This noise can be reduced for weekly mean data, which may then lead to a reduction of the sampling error in weekly estimation. This is confirmed in our calculation. Similar to the daily estimation, as the sample size is increased from 1×60 yr to 5×60 yr, 10×60 yr, 30×60 yr, 50×60 yr, and 100×60 yr, our further experiments show that the RMSE (correlation) of the ensemble mean estimation of the seasonal cycle is reduced (increased) from 0.23 (~0.4) to 0.11 (0.76), 0.085 (0.86), 0.06 (0.94), 0.06 (0.96), and 0.05 (0.97), respectively. For a single sample of 60 yr, Fig. 1b shows the direct estimation of the weekly feedback coefficient. The sampling error (annual mean ensemble spread) is now slightly reduced

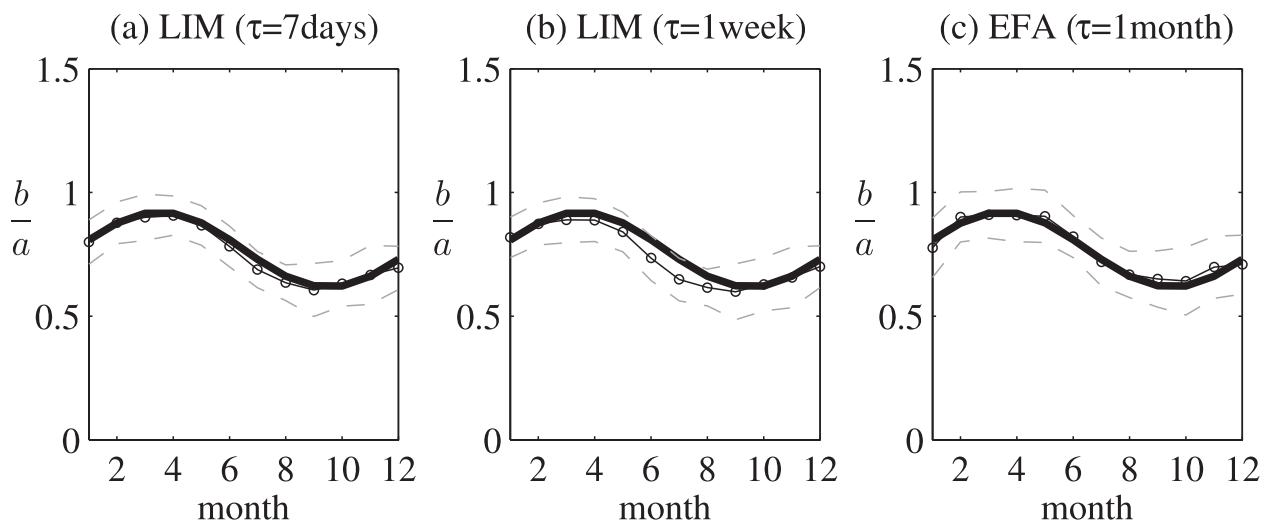## (a) LIM (τ=7days) (b) LIM (τ=1week) (c) EFA (τ=1month)

FIG. 2. As in Fig. 1, but for the feedback estimation as a function of calendar month. Shown are the LIM estimation of monthly feedback using the indirect method with (a) daily and (b) weekly data and (c) the monthly GEFA estimation.

from the daily estimation of 0.28 to 0.20 but is still larger than the amplitude of the seasonal cycle 0.15.

One might expect a further reduction of the sampling error for the direct estimation using monthly data, because of the further reduction of the noise in the monthly mean data. However, the direct monthly estimation shows a significant increase of the sampling error over the weekly and even daily estimation (Fig. 1c), with the annual mean ensemble spread being 1.31. Further experiments show that this RMSE (correlation) of the ensemble mean is reduced (increased) only modestly from about 0.38 (0.56) to 0.22 (0.87) when the sample size increases from 1×60 yr to 100×60 yr. Therefore, even with 50–100×60 yr, the estimation still shows significant bias from the truth, with an RMSE ~ 0.22. The failure of the direct monthly estimation is largely due to the fundamental nature of LIM. As discussed in Part I (Penland and Sardeshmukh 1995), in LIM, the atmospheric response depends critically on the lagged covariance of the rapid fluctuations of the atmospheric dynamics [as in Eq. (3.1a)]. A monthly mean tends to filter out the rapid atmospheric fluctuation, leaving only the quasi-equilibrium response [as in (2.2)]. Therefore, the lagged covariance in LIM is no longer able to capture the rapid atmospheric responses. For the same reason, the direct LIM estimation of seasonal data further deteriorates.

To best estimate the monthly and seasonal feedback coefficients in LIM, we therefore use an indirect method. We first calculate the covariance using the direct method in daily (weekly) data, and the covariances estimated using daily (weekly) data are then averaged to each calendar month. We speculate that this indirect method will give good estimation of monthly feedback coefficients,

because this method maintains the lagged covariance of rapid fluctuations as in the direct daily and weekly estimation and, in the meantime, reduces the sampling error with the monthly mean.

Our speculation is confirmed in Fig. 2a, which shows an example of the indirect method with the monthly mean on the direct daily estimation. Compared with the direct daily estimation in Fig. 1a, the indirect method reduces the sampling error for a sample size of 60 yr significantly, with the sampling error (annual mean ensemble spread) reduced from 0.28 in the direct method to 0.089. Further calculation with larger sample sizes show that the RMSE (and correlation) of the indirect of the length of 60 yr is better than that of the direct method of 10 times longer sample size. The improved estimation of the indirect method also applies to the weekly data. The same indirect estimation but with the monthly mean on the direct weekly estimation (as in Fig. 1b) largely reduces the sampling error from the direct method of 0.20 to 0.09, giving a similar monthly estimation (Fig. 2b) as from the indirect daily estimation (Fig. 2a), both improved over the direct weekly estimation (Fig. 1b). Therefore the indirect estimation of the monthly feedback parameter, using either daily or weekly data, appears to be the optimal approach.

As discussed in Part I for the stationary case, the lag of optimal estimation should be longer than the atmospheric response time. Figure 3a shows the correlation and RMSE (relative to the truth) of the estimated seasonal cycle with the truth as a function of the lag of LIM estimation. The seasonal cycle is estimated for the monthly feedback parameter $B = b/a$ using the indirect method averaged with daily data, and a 50 member of ensemble is
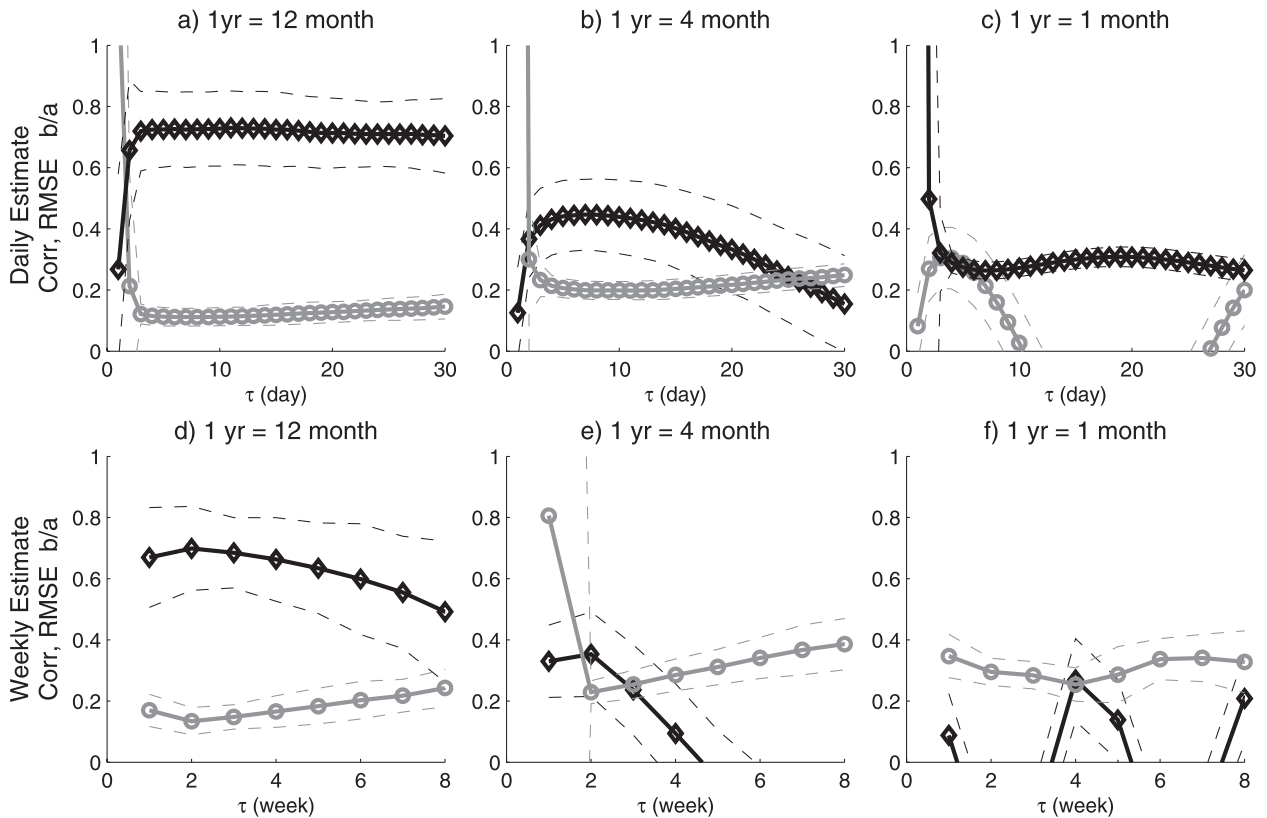
FIG. 3. LIM estimation of the seasonal cycle of the feedback parameter b/a using the indirect method (as in Fig. 2) using (a)–(c) daily and (d)–(f) weekly data in the idealized model. The length of one nominal year is (a),(d) 12 months; (b),(e) 4 months; and (c),(f) 1 month. Each panel shows the correlation (black diamonds) and RMSE (normalized relative to the truth) (gray circles) of the seasonal cycle estimated at different lags against the truth (negative correlations are not drawn). For each nominal year, the correlation and RMSE are calculated using 12 nominal months, which equals 1/12th of a nominal year. To ensure the same sample size of the average for each nominal month in the indirect method, the ensemble sizes are taken as 50, $50 \times 3 = 150$, and $50 \times 12 = 600$ for a nominal year of 12 months, 4 months, and 1 month, respectively. As a result, the feedback for one nominal month is derived from 1500 daily estimates for all the three cases ($= 30$ days $\times 50$ members $= 10$ days $\times 150$ members $= 3$ days $\times 600$ members). The ensemble mean and ensemble spread are plotted as the heavy solid lines (with marks) and thin dashed lines, respectively.

used, each of 60 yr (as in Fig. 2a). It is seen that the seasonal cycle is estimated well for lags longer than the atmospheric response time, ~3 days, with a correlation ~0.7 ± 0.1 and RMSE ~0.1 ± 0.01 (0.1 = 10% of the truth). Using the weekly data (as in Fig. 2b), the optimal estimation is achieved at the lag of 2 weeks, with a correlation of ~0.7 ± 0.12 and RMSE of ~0.1 ± 0.02 (Fig. 3d), comparable with that using the daily data (Fig. 3a). The estimation degenerates for too large lags because of the reduced sample size, as for the time-independent case discussed in Part I.

The success of LIM on seasonal cycle is not obvious. If the time scale of the time-dependent coefficients in the coupled system (2.1a) and (2.1b) is longer than the time scale of the ocean, the entire coupled system can be treated as a system of slowly varying coefficient. The optimal solution (2.10a) and (2.10b) should still be valid

approximately, and then, obviously, LIM is still valid. However, the annual cycle, although much slower than the atmospheric time scale, is of comparable time scale with the oceanic time scale. Now, it is not obvious how good the approximation the optimal solution (2.10b), and in turn the LIM estimator (2.11b) is, in particular, for a finite sample size.

Our discussion above does suggest that the LIM estimation of seasonal cycle should degenerate as the length of the annual cycle is reduced, because of the reduced separation of time scales. Figure 3b shows the correlation and RMSE of the estimated seasonal cycle is the same as in Fig. 3a, but for a nominal year of the length of 4 months. The ensemble mean correlation is reduced from 0.7 in Fig. 3a to less than 0.5, and the RMSE is increased from 0.1 to >0.2. Furthermore, the lag range for the optimal estimation is reduced from 3–40 days to
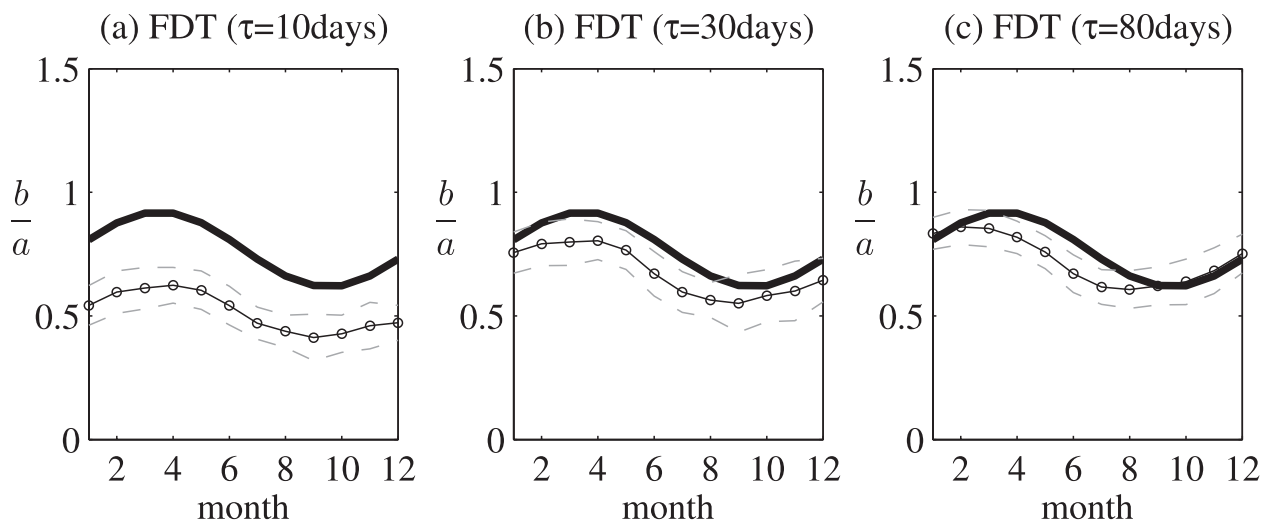
FIG. 4. FDT estimation of the seasonal cycle of the feedback for each calendar month using the indirect method in daily data in the idealized model. Shown are the results for different integration upper bound: (a) tau = 10 days, (b) tau = 30 days, and (c) tau = 80 days. The line legends are as in Figs. 1 and 2.

5–10 days. As the length of a nominal year is reduced to 1 month, the estimated seasonal cycle is much further degenerated, with the correlation reduced to less than 0.3 and even negative, the RMSE increased to over 0.3, and an even narrower range of lags for optimal estimation (Fig. 3c). Similarly, the degenerated seasonal cycle with the length of the nominal annual cycle is also seen for weekly data estimation, in comparing Figs. 3e,f with Fig. 3d.[3]

b. Comparison with GEFA and FDT

The seasonal cycle of monthly feedback coefficient is also estimated using GEFA (Fig. 2c). As discussed in section 2, GEFA makes uses of the quasi-equilibrium responses and use the monthly data to calculate the covariance in (2.6). The GEFA estimation (Fig. 2c) is of comparable accuracy (with the annual mean ensemble spread being 0.11) as the indirect LIM estimations in

Fig. 2a (spread 0.089) and Fig. 2b (spread 0.092). Therefore, GEFA and LIM can give good estimation of monthly feedback with comparable accuracy. This is similar to the annual mean response in Part I.

In comparison, FDT tends to produce a bias in the phase of the seasonal cycle. Figure 4 shows the monthly feedback parameter estimated using a FDT that is similar to the indirect method of LIM shown in Fig. 2a. That is, the feedback for each calendar day is estimated first using daily data as in (2.17), and the daily feedback coefficients are then averaged for each calendar month. Figure 4a shows the FDT estimation with a short integration upper bound [in (2.12)] of 10 days. The short integration in Fig. 4a shows an underestimation of the overall feedback strength and a slight underestimation of the amplitude of the seasonal cycle. This bias is reduced somewhat when the integration upper bound is increased to 30 days (Fig. 4b). As the integration time is increased further to 80 days (Fig. 4c), the biases in the overall feedback strength and the amplitude of the seasonal cycle are further reduced. However, the seasonal cycle is shifted earlier by ~2 months. This example shows an intrinsic problem in the FDT estimation of the seasonal cycle. For a time-independent feedback, the FDT Eq. (2.12) shows that, in principle, the FDT estimation should be integrated toward infinity. In practice, with a given sample size, the covariance with large lags comparable with the sample size tends to have large sampling errors. Therefore, as discussed in Part I, the FDT estimation is always improved when the integration length is increased (as long as it is much shorter than the sample length). In the case of seasonally varying feedback,

---

[3] Regardless of the sampling error, however, one may speculate that the success of LIM depends on the annual cycle being much longer than the rapid atmospheric response time, instead of the slow oceanic time scale. This is because the success of LIM in estimating the feedback parameter $B = b/a$ depends on the estimation of the coefficients in the atmospheric Eq. (3.1a) (a and b), instead of the oceanic Eq. (3.1b). This speculation is confirmed with our further experiments of sufficiently large sample sizes. It is found that, even with a nominal year as short as 2–3 months, relative to the truth, the estimated seasonal cycle has a correlation of ~0.8–0.9 and an RMSE of <0.1 (e.g., the ensemble mean estimation in Figs. 1a,b), although the lag range for best estimation is reduced significantly similar to Fig. 3 (not shown).
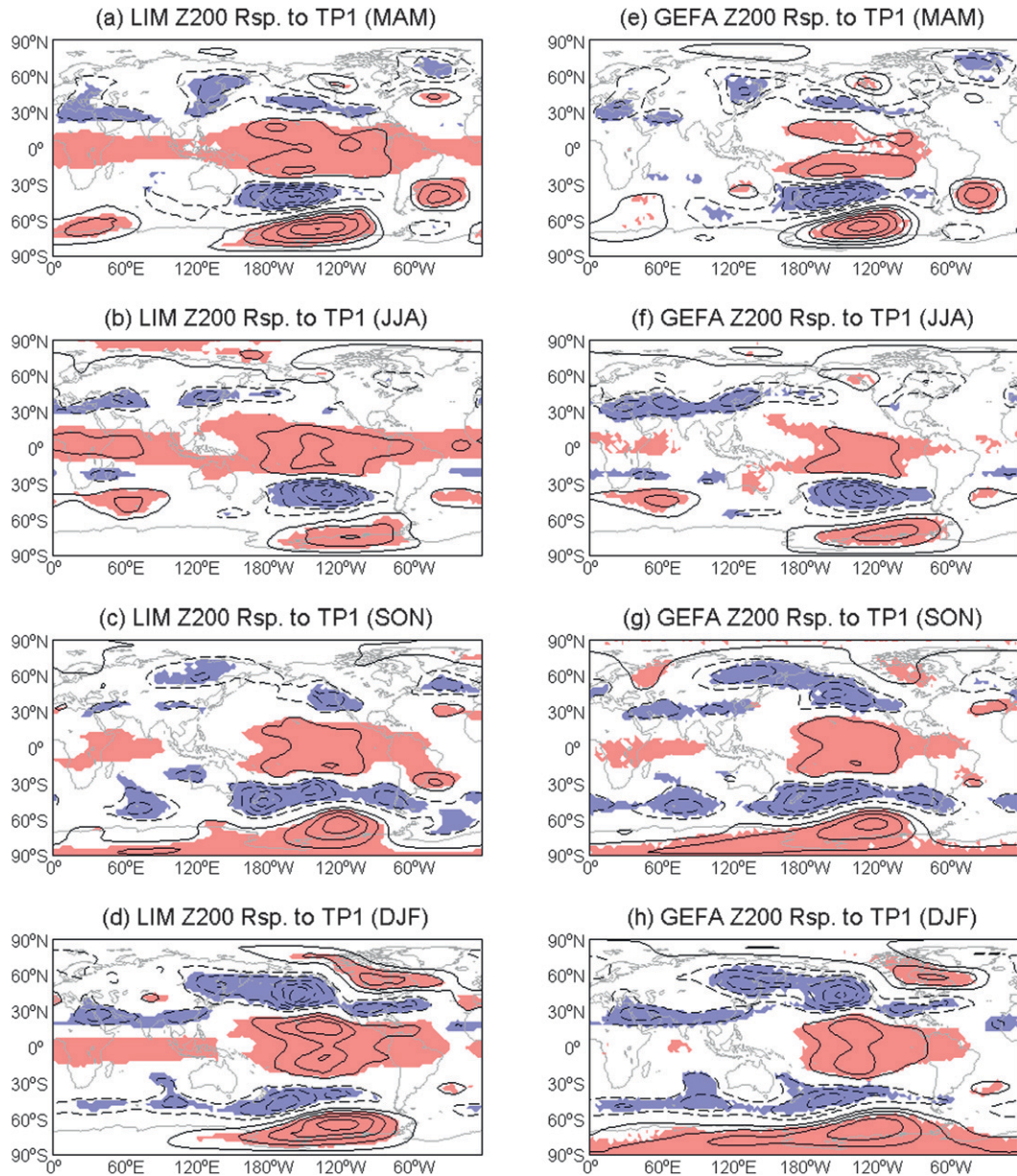
FIG. 5. Comparison between (a)–(d) weekly LIM and (e)–(h) monthly GEFA responses for Z200 to ENSO mode in the TP (TP1). Solid (dashed) contours are for positive (negative), with the interval being equal to 10 gpm (zero line omitted), and the region above 95% confidence level is shaded in red for positive and in blue for negative. The magnitude of the response should be interpreted as that to the same SST EOF1 pattern that has a maximum SST anomaly in the eastern equatorial Pacific of 1.1°C.

however, a longer integration time—although it improves the FDT in the strength of the feedback—introduces feedback signals from other calendar months. This produces a systematic shift of the seasonal cycle. Therefore, even though FDT can be as accurate as LIM and GEFA for the annual mean feedback (see Part I), the seasonal cycle of the feedback is best estimated using LIM and GEFA.

4. Observational study

We now compare GEFA and LIM for the atmospheric response to SST variability in observations. The atmosphere observations are from the National Centers for Environmental Prediction–National Center for Atmospheric Research (NCEP–NCAR) reanalysis of 1948–2010 (http://www.esrl.noaa.gov/psd/data/gridded/

TABLE 1. Cross pattern correlation between the GEFA (lag = 1 month) and LIM (lag = 3 weeks) responses to TP1 in all the seasons.

	LIM/MAM	LIM/JJA	LIM/SON	LIM/DJF	GEFA/MAM	GEFA/JJA	GEFA/SON	GEFA/DJF
LIM/MAM	1							
LIM/JJA	0.57	1						
LIM/SON	0.63	0.44	1					
LIM/DJF	0.67	0.41	0.61	1				
GEFA/MAM	**0.95**	0.60	0.58	0.65	1			
GEFA/JJA	0.61	**0.94**	0.48	0.44	0.63	1		
GEFA/SON	0.68	0.48	**0.94**	0.72	0.63	0.53	1	
GEFA/DJF	0.66	0.44	0.71	**0.91**	0.61	0.51	0.83	1

data.ncep.reanalysis.html), daily, 2.5° × 2.5° global grids (144 longitudes × 73 latitudes). SST data are monthly Hadley Centre Sea Ice and SST dataset (HadISST) data (http://www.opsi.gov.uk/advice/crown-copyright/copyright-guidance/index.htm). For weekly LIM (and GEFA; see appendix) assessment, we obtain the weekly SST using a cubic spline interpolation from the monthly SST. [Similar results are obtained using the weekly average of the daily skin temperature (SKT) (not shown)]. All the data are anomalies from the seasonal cycle and are detrended by a third-order polynomial. Similar to Wen et al. (2010, hereafter W10) and Part I, we will study the response of the 200-hPa geopotential height (Z200) to the dominant SST EOF modes but now focusing on the comparison of seasonal responses estimated in the monthly GEFA and weekly LIM. The SST EOFs, which are derived from the year-round SST variability, are used to represent the SST forcing because they are often used as the definition of major SST variability modes. Furthermore, the EOF base for SST forcing reduces the correlation among different forcings and therefore reduces sampling error significantly (Fan et al. 2011).

In our study here, each principal component (time series of EOF expansion coefficient) is standardized for the year-round variability ($\sigma = 1$) and the dimensional magnitude is represented in each EOF pattern. As such, the atmospheric response is interpreted as the response to each dimensional EOF. A total of 10 SST modes are used, which are the first two regional EOFs in the tropical Pacific (TP; 20°S–20°N, 120°E–60°W), tropical Indian Ocean (TI; 20°S–20°N, 35°–120°E), tropical Atlantic (TA; 20°S–20°N, 65°W–15°E), North Pacific (NP; 20°–60°N, 120°E–60°W) and North Atlantic (20°–60°N, 100°W–20°E). As in W10 and Part I, our results are insensitive to the choice of the ocean regions and the truncation number of leading EOF modes. The indirect LIM assessment is the seasonal mean of the direct weekly LIM estimation. The estimation has some variations with lags of estimation (see appendix). Here, we chose the weekly LIM of lag = 3 weeks. A tau test (Penland and

Sardeshmukh 1995; Shin et al. 2010) similar to that in Part I (appendix B there) shows that these LIM responses are not very sensitive to lags, especially its response pattern (see appendix). The GEFA assessment uses monthly data at the lag = 1 month and is averaged for each season. Monthly GEFA at a larger lag has similar response pattern, but it tends to have a larger magnitude due to the decorrelation of SST (W10) and is subject to higher sampling error (Liu et al. 2006). The statistical significance for both LIM and GEFA is tested with a Monte Carlo method, in which the atmospheric field is randomly scrambled 100 times.

We will show the comparison of LIM and GEFA assessments for the seasonal responses to the first EOFs of the tropical Pacific (TP1; the ENSO mode), the tropical Indian Ocean [TI1; the Indian Ocean basin (IOB) mode], and the North Pacific [NP1; the North Pacific Oscillation (NPO) mode] (see Fig. 1 of W10 for their patterns). Part I has shown that the annual mean responses are consistent in LIM, FDT, and GEFA with global pattern correlations of ~0.95 and global mean amplitudes comparable within about ±10%. Here, we further show that the seasonal responses are also largely consistent between GEFA and LIM.

Figure 5 shows that the overall global seasonal responses to the ENSO mode (TP1) are largely consistent in LIM and GEFA. The seasonal responses are presented in four pairs for boreal spring [March–May (MAM)], summer [June–August (JJA)], fall [September–November (SON)], and winter [December–February (DJF)] (Fig. 5). The magnitude for each response should be interpreted as the response to the TP1, which is characterized by a warming in the tropical Pacific (see Fig. 1a of W10) with a maximum SST anomaly of 1.1°C in the eastern equatorial Pacific. Here, we note that the difference in the response magnitude in different seasons is not due to the different strength of SST forcing, because the response for different seasons estimated here are subject to the same TP1 forcing. As in the annual mean response in GEFA (W10) and LIM (Part I), all the seasonal responses are dominated by a ridge locally over the eastern

FIG. 6. As in Fig. 5, but for the Z200 response to the IOB mode of the TI (TI1). The magnitude of the response should be interpreted as that to the same broad SST EOF1 pattern that has a maximum SST anomaly in the TI of 0.29°C.

equatorial Pacific and significant remote responses in the extratropics via atmospheric teleconnection.

More important here is that major differences between the responses of different seasons are also largely consistent between GEFA and LIM. As seen in Fig. 5, the two methods give comparable amplitude of response to the same magnitude of SST forcing. For the same magnitude of TP1 forcing, the strongest response occurs in winter and spring (Fig. 5) in both methods. If the magnitude of the PC1 is considered ($\sigma = 1.15$, 1.13, 0.8,

and 0.88 for fall, winter, spring, and summer), the actual seasonal atmospheric response, which can be derived by multiplying the values shown in Fig. 5 by the σ of the season. The strongest overall global response occurs in boreal winter in both methods, consistent with the peak response in the mature phase of ENSO. Furthermore, the global pattern of the response is largely consistent between LIM and GEFA, with the global pattern correlations of 0.95, 0.94, 0.94, and 0.91 for spring, summer, fall, and winter, respectively. These correlations between

TABLE 2. Cross pattern correlation between the GEFA (lag = 1 month) and LIM (lag = 3 weeks) responses to TI1 in all the seasons.

	LIM/MAM	LIM/JJA	LIM/SON	LIM/DJF	GEFA/MAM	GEFA/JJA	GEFA/SON	GEFA/DJF
LIM/MAM	1							
LIM/JJA	0.51	1						
LIM/SON	0.27	0.20	1					
LIM/DJF	0.35	0.22	0.42	1				
GEFA/MAM	**0.84**	0.64	0.14	0.21	1			
GEFA/JJA	0.54	**0.92**	0.28	0.18	0.71	1		
GEFA/SON	0.34	0.42	**0.77**	0.68	0.18	0.37	1	
GEFA/DJF	0.36	0.25	0.45	**0.90**	0.16	0.14	0.76	1

the two methods are substantially higher than the correlations between different seasons using the same method (values in boldface in Table 1). Therefore, the different features of the seasonal responses are identified with reasonable confidence in both GEFA and LIM. More specifically, the local ridge response over the eastern equatorial Pacific is the strongest in boreal winter (Figs. 5d,h). The remote Pacific North America (PNA) teleconnection into the Northern Hemisphere (NH) is present mainly in boreal winter (Figs. 5d,h) and spring (Figs. 5a,e), consistent with Kumar and Hoerling (1998). However, the Pacific South America (PSA) teleconnection into the Southern Hemisphere (SH) is present in almost all the seasons. A full understanding of the physical mechanism of these seasonal responses is beyond the scope of this study. Nevertheless, we give some brief discussions here. The strong equatorial ridge response represents perhaps a stronger atmospheric convection in boreal winter (Matsuno 1966; Gill 1980) when the seasonal warming reaches its mature phase in the eastern equatorial Pacific (Rasmusson and Carpenter 1982). The strong PNA in boreal winter and early spring is likely the result of strong westerly jet and in turn a stronger stationary wave response (Davis and Benkovic 1994; Kumar and Hoerling 1998; Notaro et al. 2006). The presence of PSA in all the seasons is somewhat unexpected. To confirm its robustness, we made a composite analysis of the ENSO years for both boreal winter and summer. It is clear that PSA exists in both winter and summer, whereas PNA exists only in winter. The presence of year-round atmospheric teleconnections in the extratropical SH seems to be consistent with previous observations (Mo and White 1985; Berbery et al. 1992; Kousky and Bell 1992) and can be attributed to the presence of waveguide there (Ambrizzi et al. 1995). We speculate that the presence of the year-round PSA is due to a weak seasonality in the SH westerly jet and in turn the stationary wave response all year-round. This speculation appears to be consistent with a recent two-layer model study (Lee et al. 2009). This study shows that, under the observed climatological wind, a tropical heating can induce

strong PNA and PSA in the respective winter as in the observation. Furthermore, the tropical heating can also force a modest PSA in austral summer but no PNA in boreal summer (their Fig. 7). A visual inspection of the climatological wind (their Fig. 6) shows that the summer barotropic westerly is less than half of that in winter in the NH but amounts to $\frac{2}{3}$ of that in winter in the SH. In addition, the summer baroclinic westerly (vertical shear) has its maximum latitude closer to the equator in the SH (DJF at 28°S) than in the NH (JJA at 45°N). Therefore, in austral summer in the SH, the baroclinic jet extends into the tropics and is able to convert tropical heating-induced baroclinic disturbance into barotropic disturbance; this barotropic disturbance then propagates through the stronger barotropic jet deep into the high-latitude SH.

Similar to the response to ENSO, the overall global seasonal response to the IOB mode (TI1) is also largely consistent between GEFA and LIM (Fig. 6). The IOB mode (TI1) is characterized by a basinwide warming over the tropical Indian Ocean with the maximum warming of 0.29°C (see Fig. 1b of W10). This mode lags the ENSO mode by about a season (with the magnitude of the PC as $\sigma = 1.13, 1.10, 0.87$, and 0.85 for winter, spring, summer, and fall, respectively), largely reflecting its passive response to ENSO (Yang et al. 2007). First, as in the year-round responses in GEFA (W10), the responses to the IOB mode is dominated by a zonally uniform ridge response around the global tropics in all the seasons in both LIM and GEFA. This is in sharp contrast to the tropical response to ENSO mode, which is dominated by a local response over the eastern Pacific (Fig. 5). Most important here, many features of the seasonal responses are common in both LIM and GEFA. The global pattern correlation between GEFA and LIM response to TI1 in all the seasons is ~0.8–0.9, substantially higher than the correlation with other seasons (values in boldface in Table 2). The correlation between summer and winter are almost zero in the same method or different methods, indicating dramatic changes in the seasonal response. The tropical response, including its circumglobal feature, is
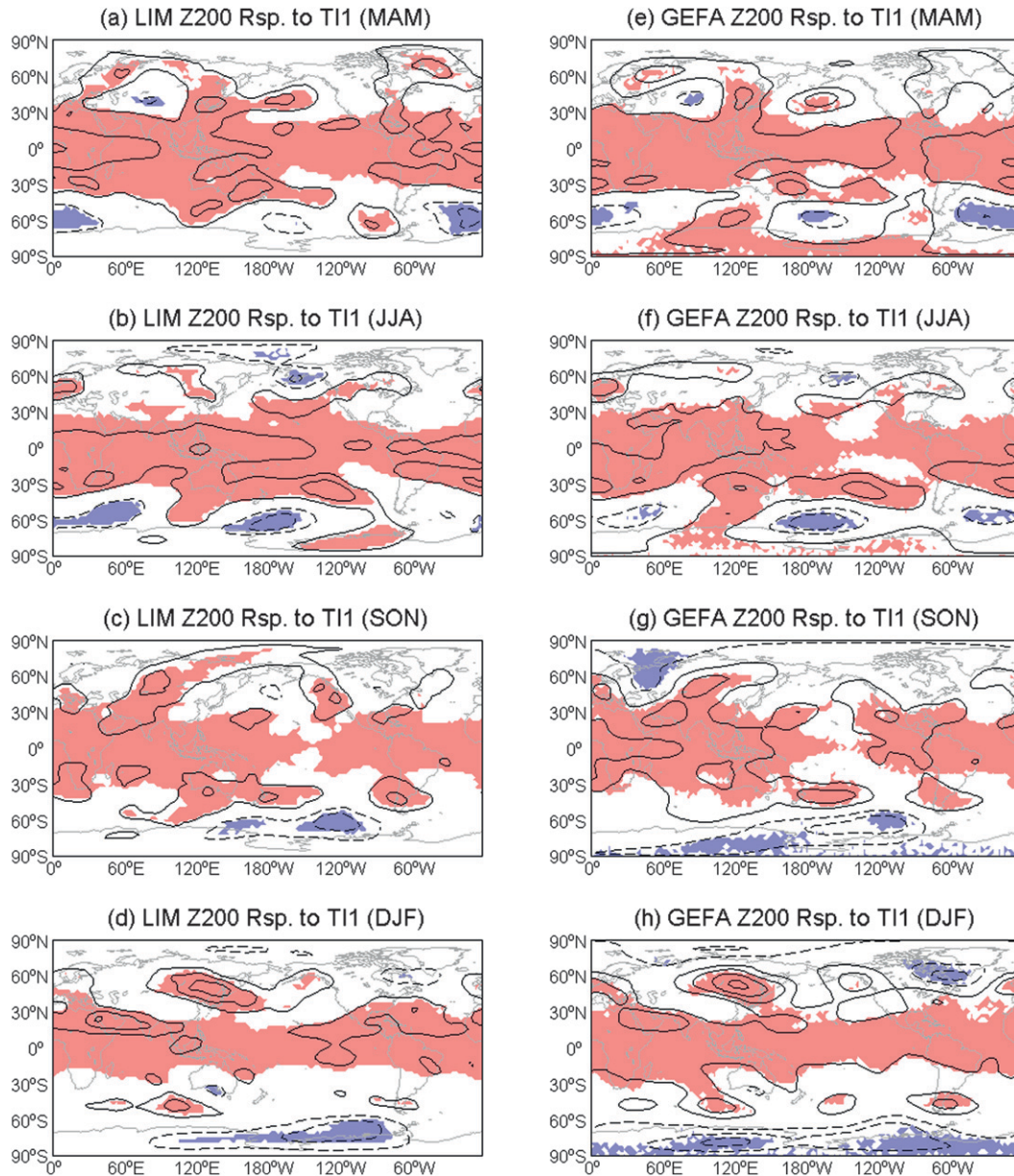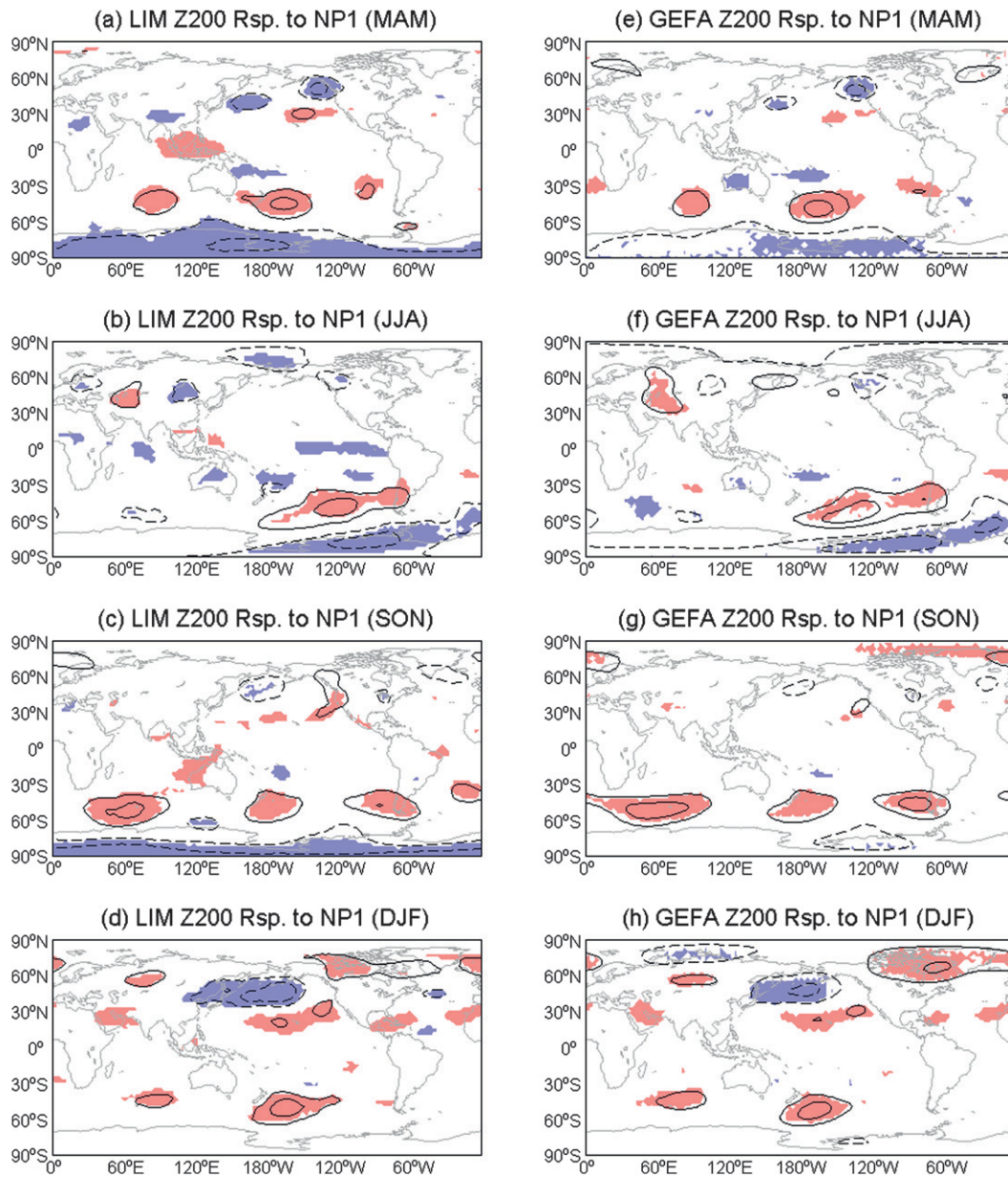
FIG. 7. As in Figs. 5 and 6, but for the Z200 response to the NPO mode in the NP (NP1). The magnitude of the response should be interpreted as that to the same SST EOF1 pattern that has a maximum negative SST anomaly in the midlatitude NP of $-0.6°C$.

the strongest in spring (Figs. 6a,e; further amplified by the large $\sigma = 1.10$) and weakest in fall (Figs. 6b,f). The mechanisms for these seasonal responses remain to be explored.

Finally, the overall global seasonal responses to the NPO mode (NP1) are also largely consistent in GEFA and LIM (Fig. 7). The NPO mode is characterized by a cold SST in the western-central North Pacific with a maximum amplitude of $-0.6°C$, surrounded by an arch

of warm SST with a maximum of $0.6°C$ (Fig. 1d of W10), which varies little with season ($\sigma \approx 1$ for all the seasons). As in the year-round response (W10; Part I), a common response in all the seasons is an enhanced Aleutian low locally over the cold North Pacific. The response to NP1 shows significant differences in seasonal responses. Most important here, these seasonal differences are common in both LIM and GEFA, as in the seasonal responses to TP1 and NP1. The seasonal responses between the two

TABLE 3. Cross pattern correlation between the GEFA (lag = 1 month) and LIM (lag = 3 weeks) responses to NP1 in all the seasons.

	LIM/MAM	LIM/JJA	LIM/SON	LIM/DJF	GEFA/MAM	GEFA/JJA	GEFA/SON	GEFA/DJF
LIM/MAM	1							
LIM/JJA	0.20	1						
LIM/SON	0.58	0.25	1					
LIM/DJF	0.37	0.18	0.33	1				
GEFA/MAM	**0.94**	0.35	0.56	0.40	1			
GEFA/JJA	0.30	**0.90**	0.38	0.11	0.45	1		
GEFA/SON	0.52	0.27	**0.85**	0.44	0.52	0.33	1	
GEFA/DJF	0.46	0.24	0.41	**0.87**	0.53	0.22	0.53	1

methods have a pattern correlation of ~0.9, substantially higher than the correlation with the responses in other seasons (values in boldface in Table 3). The response patterns are virtually uncorrelated between summer and winter in both methods, again, indicating a dramatic seasonality of the atmospheric response. More specifically, the local low pressure response and its extension into the East Asia is the strongest in winter (Figs. 7d,h). The remote response over the North Atlantic sector is the strongest in winter, dominated by a teleconnection of a high over northern Canada and a low over the North Atlantic in winter (Figs. 7d,h). The strong cold SST–low pressure response over the North Pacific in winter is consistent with previous studies in the observation and model experiments (e.g., Liu et al. 2007). The emergence of the Aleutian low–Icelandic low teleconnection in the winter is also consistent with the synoptic analysis and is associated with Rossby wave propagations (Honda et al. 2001).

Although LIM and GEFA estimation gives an overall consistent global response, it is important to point out that there are also differences between the two estimations, especially for the magnitude in specific regions; for example, the high response over Northern Canada to the Arctic is stronger in GEFA (Fig. 7h) than in LIM (Fig. 7d). The difference between the two methods can be related to a more general issue in both methods: how to choose the optimal lag for estimation. As discussed in the appendix, each method of estimation has some dependence on the lags. In particular, the magnitude of the response tends to increase with the lag, especially in GEFA. There is no perfect way for choosing the lag. An empirical rule, as suggested by Part I, is to examine the successive pattern correlation and ratio of magnitude of the response and to select the lags of more responses (i.e., successive pattern correlation close to 1 with least change of amplitude). If one uses this empirical rule, the optimal lag can differ among different seasons, in different methods, and for the responses in different regions and to different modes. Our choice of a 3-week lag for LIM here is based roughly on our empirical rule for

the global response. For the monthly GEFA, the 1-month lag is the minimum lag, chosen partly for its small sampling error (Liu et al. 2006) and partly for its lose consistency with the weekly GEFA estimation of the optimal lags of 3–4 weeks. This introduces uncertainties in the estimated response, especially in its regional amplitude. Therefore, if one is interested in the response of a specific region, we believe it is important to examine the lag dependency of that region carefully before determining the optimal lag of estimation.

In short, LIM and GEFA give largely consistent seasonal responses for all the seasons and therefore can serve for the cross validation of the seasonal atmospheric responses. Indeed, for the 40 pairs of atmospheric responses (10 SST EOF modes and four seasons), the global pattern correlation between the corresponding LIM and GEFA responses are between 0.77 and 0.96, with the average being 0.9. The amplitude ratio between LIM and GEFA responses, measured by the standard deviation of the global response, ranges from 0.77 to 1.38, with an average of 1.03. In spite of the largely consistent response from the global perspective, there are some important discrepancies in some extratropical regional responses, especially in the response magnitude. Further careful studies are needed to assess the magnitude of the regional response. In addition, the physical mechanisms of the identified seasonal responses also remain to be fully understood.

5. Summary and discussion

As an extension of Part I, we compared three statistical methods for the assessment of the seasonal cycle of the atmospheric response in both a conceptual climate model and the observation. It is found that both LIM and GEFA are able to reproduce the major features of the seasonal response over the globe. The FDT method, however, tends to produce a shift in the seasonal cycle. The capability for GEFA and LIM to assess the seasonal response appears to be due to the slow annual cycle time scale relative to the rapid atmospheric
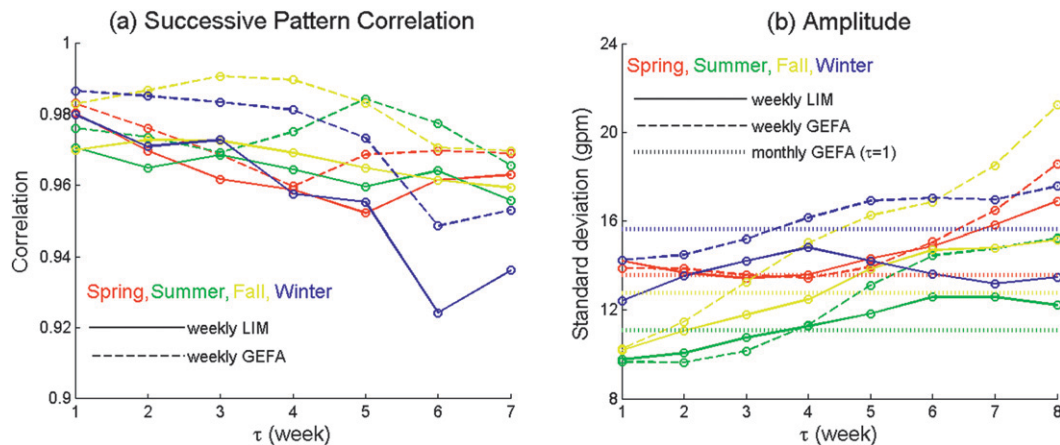
FIG. A1. (a) Successive pattern correlation of the global seasonal responses to TP1 mode estimated at different lags (in weeks) in weekly LIM (solid) and weekly GEFA (dashed). The successive correlation at lag n represents the pattern correlation between lag n and lag $n + 1$. (b) The magnitude (spatial standard deviation) of the global responses to TP1 estimated at different lags for weekly LIM (solid) and GEFA (dashed). In (b), the monthly GEFA responses at lag 1 month are also plotted as the constant (dotted) lines. Color schemes are red for spring, green for summer, yellow for fall, and blue for winter.

response time. Therefore, GEFA and LIM can be used to provide independent assessment of the seasonal atmospheric response in the observation. Finally, much effort is still needed to assess the magnitude of regional responses and to understand the mechanism of the atmospheric response.

APPENDIX

Observational Responses Estimated at Different Lags

We have examined the seasonal response in observations using weekly LIM, weekly GEFA, and monthly GEFA at various lags. The major features of the estimated global responses are robust. In particular, consistent with the annual responses discussed before (Liu et al. 2008; W10; Part I), the pattern and magnitude of the seasonal global responses tend to be stable. As an example, here we only show the response to the Pacific ENSO mode (TP1) using the SST forcing that is the same as in Figs. 5–7. [The major results are similar for the response to TI1 and NP1 (not shown).]

Figure A1a shows the successive pattern correlation of the global seasonal responses in weekly LIM and weekly GEFA of lags 1–8 weeks. It is seen that almost all the pattern correlations are above 0.95. A more comprehensive view of the pattern can be seen in Fig. A2, which shows the pattern cross correlation among all the weekly GEFA, LIM, and the 1-month GEFA. The first feature is that weekly LIM and weekly GEFA are highly correlated for all the seasons, in particular at the same lag (diagonal; correlation > 0.95). Indeed, unless the lags are very different (e.g., >4 weeks), all the patterns in GEFA and LIM are correlated close and above 0.9. Furthermore, except for lags larger than 7 in some seasons, weekly LIM are highly correlated with the monthly GEFA (correlation close and higher than 0.9), with the highest correlation at lags close to 1 month (3, 4, and 5 weeks).

The response magnitude has features similar to the pattern correlation but with somewhat larger uncertainty. Figure A1b shows the magnitude of the global seasonal response (in spatial standard deviation) in weekly LIM and weekly GEFA for lags 1–8 weeks. For reference, the monthly GEFA response at lag 1 month is also shown. First, the magnitude of the global response tends to increase with the lag, especially in GEFA. This increase of magnitude in GEFA is caused by the decorrelation of SST forcing as discussed before (Liu et al. 2008; W10; Part I). The magnitudes vary by ~10%–20% for LIM but larger for GEFA especially for fall and spring. Similar to the pattern correlation, the magnitude of the weekly estimation is closest to the monthly GEFA (1 month) around the lags 3 and 4 weeks (similar to the pattern correlation). A comprehensive view of the magnitudes

Cross Pattern Correlation of GEFA and LIM (TP1)
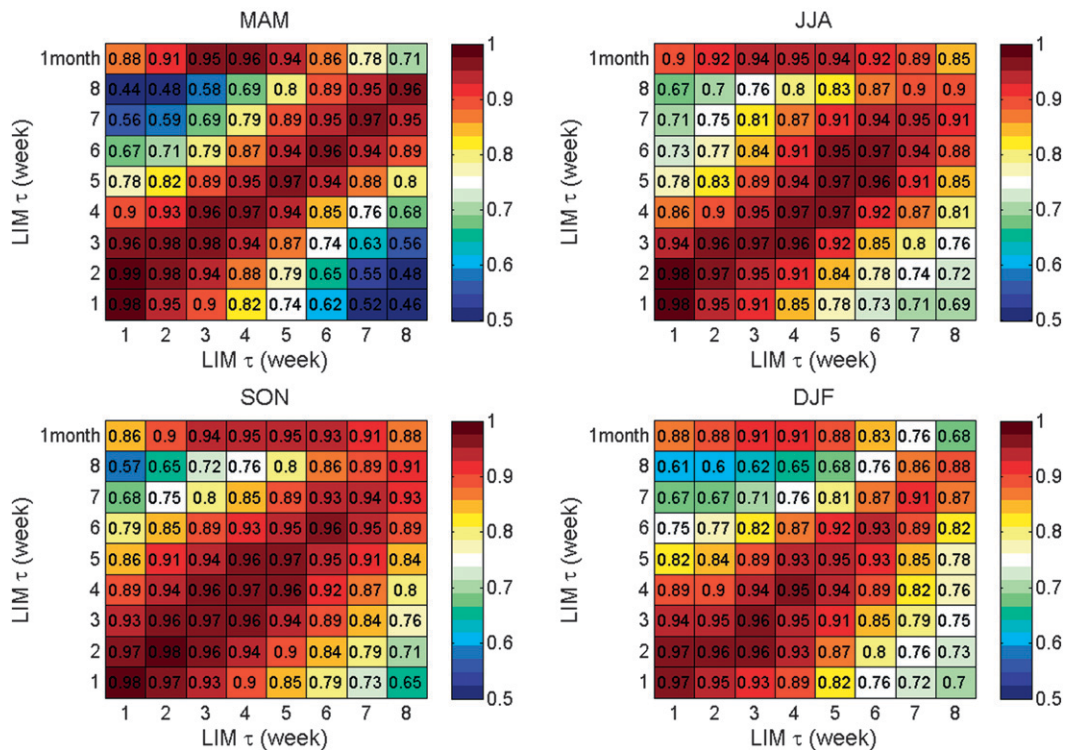
FIG. A2. Pattern correlation of the global response to TP1 between weekly GEFA and weekly LIM estimated at lags 1–8 weeks for the four seasons. For each season, the vertical axis is the lag (in weeks) for GEFA and the horizontal axis is the lag (in weeks) for LIM; (top) the correlation between weekly LIM and the monthly GEFA (lag 1 month).

can be seen in the cross ratios of the magnitude in Fig. A3. First, as seen in Fig. A1b, the magnitude of LIM and GEFA responses tend to increase with lags (for each column and row, respectively). Second, GEFA and LIM tend to have comparable magnitude with a ratio close to one, especially for comparable lags (along the diagonal). LIM estimation has a comparable magnitude to the monthly GEFA at lags 3–4 weeks.

The variation of the response with lag makes it difficult to choose the optimal lag for estimation. In particular, the highest successive pattern correlation occurs at different lags for different season and in different methods (Fig. A1a). From our empirical rule (Part I),

this implies the optimal lag should be different for different season and different methods. In the paper (Figs. 5–7), for simplicity and from the overall global perspective, we have used the weekly LIM at lag 3 because this lag has a rather high successive correlation for most seasons. This lag is also consistent with our annual mean estimation in Part I. The monthly GEFA (at month 1) is used because it is the simplest monthly GEFA estimation and seems to be not too different from the optimal weekly estimation (at lags 3–4 weeks). One can further imagine that, for the response at different regions, the optimal lag will also be different and therefore requires further studies.

Stand deviation ratio (TP1, ratio of GEFA to LIM)

FIG. A3. Ratio of the magnitude of global response to TP1 between weekly GEFA and weekly LIM estimation [std(GEFA)/std(LIM)] of lags 1–8 for the four seasons. For each season, the vertical axis is the lag (in weeks) for GEFA and the horizontal axis is the lag (in weeks) for LIM; (top) the ratio between monthly GEFA (lag 1 month) and weekly LIM.

REFERENCES

Alexander, M. A., L. Matrosova, C. Penland, J. D. Scott, and P. Chang, 2008: Forecasting Pacific SSTs: Linear inverse model predictions of the PDO. *J. Climate,* **21,** 385–402.

Ambrizzi, T., B. Hoskins, and H.-H. Hsu, 1995: Rossby wave propagation and teleconnection patterns in the Austral winter. *J. Atmos. Sci.,* **52,** 3661–3672.

Barsugli, J., and D. Battisti, 1998: The basic effects of atmosphere–ocean thermal coupling on midlatitude variability. *J. Atmos. Sci.,* **55,** 477–493.

Bell, T. L., 1980: Climate sensitivity from fluctuation dissipation: Some simple model tests. *J. Atmos. Sci.,* **37,** 1700–1707.

Berbery, E. H., I. Nogués-Paegle, and J. D. Horel, 1992: Wavelike Southern Hemisphere extratropical teleconnections. *J. Atmos. Sci.,* **33,** 1607–1623.

Blumenthal, M. B., 1991: Predictability of a coupled ocean-atmosphere model. *J. Climate,* **4,** 766–784.

Davis, R. E., and S. R. Benkovic, 1994: Spatial and temporal variations of the January circumpolar vortex over the Northern-Hemisphere. *Int. J. Climatol.,* **14,** 415–428.

Fan, L., Z. Liu, and Q. Liu, 2011: Robust GEFA assessment of climate feedback to SST EOF modes. *Adv. Atmos. Sci.,* **28,** 907–912.

Frankignoul, C., A. Czaja, and B. L'Heveder, 1998: Air–sea feedback in the North Atlantic and surface boundary conditions for ocean models. *J. Climate,* **11,** 2310–2324.

Gardiner, C. W., 1997: *Handbook of Stochastic Methods for Physics, Chemistry and the Natural Sciences.* Springer, 442 pp.

Gill, A. E., 1980: Some simple solutions for heat-induced tropical circulation. *Quart. J. Roy. Meteor. Soc.,* **106,** 447–462.

Gritsun, A., and G. Branstator, 2007: Climate response using a three-dimensional operator based on fluctuation–dissipation theorem. *J. Atmos. Sci.,* **64,** 2558–2572.

Hasselmann, K., and T. P. Barnett, 1981: Techniques for linear prediction for systems with periodic statistics. *J. Atmos. Sci.,* **38,** 2275–2283.

Honda, M., H. Nakamura, J. Ukita, I. Kousaka, and K. Takeuchi, 2001: Interannual seesaw between the Aleutian and Icelandic lows. Part I: Seasonal dependence and life cycle. *J. Climate,* **14,** 1029–1042.

Kirk-Davidoff, D. B., 2009: On the diagnosis of climate sensitivity using observation of fluctuations. *Atmos. Chem. Phys.,* **9,** 813–822.

Kousky, V. E., and G. D. Bell, 1992: *Atlas of Southern Hemisphere 500-mb Teleconnection Patterns Derived from National Meteorological Center Analyses.* NOAA Atlas 9, 90 pp.

Kumar, A., and M. P. Hoerling, 1998: Annual cycle of Pacific–North American seasonal predictability associated with different phases of ENSO. *J. Climate,* **11,** 3295–3308.

Lee, S.-K., C. Wang, and B. E. Mapes, 2009: A simple atmospheric model of the local and teleconnection responses to tropical heating anomalies. *J. Climate,* **22,** 272–284.

Leith, C. E., 1975: Climate response and fluctuation dissipation. *J. Atmos. Sci.,* **32,** 2022–2026.

Liu, Z., M. Notaro, J. Kutzbach, and N. Liu, 2006: Assessing global vegetation–climate feedbacks from the observation. *J. Climate,* **19,** 787–814.

——, Y. Liu, L. Wu, and R. Jacob, 2007: Seasonal and long-term atmospheric response to reemerging North Pacific Ocean variability: A combined dynamical and statistical assessment. *J. Climate,* **20,** 955–980.

——, N. Wen, and Y. Liu, 2008: On the assessment of nonlocal climate feedback. Part I: The generalized equilibrium feedback analysis. *J. Climate,* **21,** 134–148.

——, ——, and L. Fan, 2012: Assessing atmospheric response to surface forcing in the observations. Part I: Cross validation of annual response using GEFA, LIM, and FDT. *J. Climate,* **25,** 6796–6816.

Matsuno, T., 1966: Quasi-geostrophic motions in the equatorial area. *J. Meteor. Soc. Japan,* **44,** 25–43.

Mo, K. C., and G. H. White, 1985: Teleconnections in the Southern Hemisphere. *Mon. Wea. Rev.,* **113,** 22–37.

Newman, M., P. D. Sardeshmukh, and C. Penland, 2009: How important is air–sea coupling in ENSO and MJO evolution? *J. Climate,* **22,** 2958–2977.

Notaro, M., W.-C. Wang, and W. Gong, 2006: Model and observational analysis of the northeast U.S. regional climate and its relationship to the PNA and NAO patterns during early winter. *Mon. Wea. Rev.,* **134,** 3479–3505.

OrtizBreviá, M. J., 1997: Estimation of the cyclostationary dependence in geophysical data fields. *J. Geophys. Res.,* **102,** 13 473–13 486.

Penland, C., 1989: Random forcing and forecasting using principal oscillation pattern analysis. *Mon. Wea. Rev.,* **117,** 2165–2185.

——, and P. D. Sardeshmukh, 1995: Error and sensitivity analysis of geophysical eigensystems. *J. Climate,* **8,** 1988–1998.

Rasmusson, E. M., and T. H. Carpenter, 1982: Variations in tropical sea surface temperature and surface wind fields associated with the Southern Oscillation/El Niño. *Mon. Wea. Rev.,* **110,** 354–384.

Shin, S.-I., P. D. Sardeshmukh, and K. Pegion, 2010: Realism of local and remote feedbacks on tropical sea surface temperatures in climate models. *J. Geophys. Res.,* **115,** D21110, doi:10.1029/2010JD013927.

Wen, N., Z. Liu, Q. Liu, and C. Frankignoul, 2010: Observed atmospheric responses to global SST variability modes: A unified assessment using GEFA. *J. Climate,* **23,** 1739–1759.

Yang, J., Q. Liu, S.-P. Xie, Z. Liu, and L. Wu, 2007: Impact of the Indian Ocean SST basin mode on the Asian summer monsoon. *Geophys. Res. Lett.,* **34,** L02708, doi:10.1029/2006GL028571.